8692 *Biochemistry* **2009,** *48,* 8692–8703
DOI: 10.1021/bi901099s

BIOCHEMISTRY
including biophysical chemistry & molecular biology
Article

The Native-like Interactions between SNase121 and SNase(111−143) Fragments Induce the Recovery of Their Native-like Structures and the Ability to Degrade DNA[†,‡]

Yong Geng,[§] Yingang Feng,[§] Tao Xie, Lu Shan, and Jinfeng Wang*

National Laboratory of Biomacromolecules, Institute of Biophysics, Chinese Academy of Sciences, 15 Datun Road, Beijing 100101, China. [§] *Contributed equally to this work.*

Received June 30, 2009; Revised Manuscript Received August 5, 2009

ABSTRACT: The interactions necessary for stabilizing the folding of the N-terminal large β-subdomain and the C-terminal small α-subdomain of staphylococcal nuclease (SNase) were investigated by an approach of fragment complementation. Two SNase fragments, namely, SNase121 and SNase(111−143) containing 1−121 and 111−143 residues, respectively, of native SNase, were used in this study since the sequences of the two fragments correspond to that of the β- and α-subdomains of SNase. SNase121 is a largely unfolded fragment whereas SNase(111−143) is a structureless fragment. The recognition process and efficiency of complementation of SNase121 and SNase(111−143) fragments were studied by NMR and various biochemical and biophysical methods. SNase121 and SNase(111−143) can recognize each other and recover their native conformations on binding, restoring the active site and the ability to degrade DNA. The SNase121:SNase(111−143) complex showed a nuclease activity up to 30% that of native SNase. The final rigid structures of SNase121 and SNase(111−143) fragments having the folded native-like β-subdomain and α-subdomain structures of SNase, respectively, in the complex form simultaneously with the complex stabilization. Studies with the mutant SNase121 and SNase(111−143) fragments reveal that the sequence elements which are essential for recognition and efficient complementation of the two fragments are also necessary for recovering the native-like interactions at the binding interface between them. The interfragment interactions that induce the structural complementation of SNase121 and SNase(111−143) likely reflect the tertiary interactions necessary to stabilize the folding of both β- and α-subdomains in the native SNase.

Fragment complementation for certain single domain proteins presents as a sensitive phenomenon, that the fragments cleaved from native protein have the ability to form a folded noncovalent complex which frequently exhibits both native-like structure and function. This phenomenon was used in studies of protein folding and in analyzing the essential recognition elements for stable folding. Folding complementation of protein fragments produced by limited proteolytic cleavage or genetic methods has been studied under both *in vivo* and *in vitro* conditions (*1*−*4*). In 1959, Richards and Vithayathil reported that the mixture of two enzymically inactive components of modified ribonuclease can recover almost the full enzymic activity (*5*). In 1977, recovery of ribonuclease activity by complementation of fragments of barnase was reported. Activity is restored to barnase(l−102) by combination with barnase(99−108) or barnase(88−110) obtained from trypsin digests of native protein (*6*). In following years, more reports about fragment complementation appeared, for example, two fragments of chymotrypsin inhibitor-2 (CI-2[1]), namely, CI-2(20−59) and CI-2(60−83), associate (K_d = 42 nM) to yield a complex that has fluorescence and circular dichroism (CD) spectra identical to those of uncleaved CI-2. The recovered native-like structure of the complex showed the ability to inhibit chymotrypsin (*7*). 9 and 5 kDa fragments of the N-terminal SH2 domain from the p85α subunit of phosphatidylinositol 3′ kinase can fold into a native-like structure on binding to create a noncovalent complex, which retains limited biological activity and can bind their target peptide (*8*, *9*). Recently, it was demonstrated that the AroA enzyme and its glyphosate tolerance activities can be directly reconstituted from two separate inactive AroA fragments under both *in vivo* and *in vitro* conditions (*10*).

Staphylococcal nuclease (SNase) has been extensively studied as a model system for protein folding. An early study has reported that fragments of SNase containing residues 6−48 (SNase(6−48)) and residues 49−149 and 50−149 (SNase(49, 50−149)) were produced by trypsin in the presence of pdTp (thymidine 3′,5′-bisphosphate) and Ca^{2+}. Neither of these fragments alone showed enzymatic activity or folded structure. The association of SNase(6−48) with SNase(49, 50−149) regenerated enzymatic activity 8−10% of the activity of the native level (*1*, *11*). The approximate enzymatic activity can be restored also to the complex of SNase(1−126) with SNase(49, 50−149), SNase-(99−149) or SNase(111−149) and the complex of SNase(1−123) with SNase(114−149) isolated from trypsin digests (*12*−*14*). Two

[†]This research is supported by the National Natural Science Foundation of China (NNSFC 30570375).

[‡]The atomic coordinates and NMR restraints of SNase121:SNase-(111−143) complex have been deposited in the Protein Data Bank under ID code 2KHS. The chemical shifts of SNase121:SNase(111−143) complex have been deposited in the BioMagResBank database with accession number 15357.

*To whom correspondence should be addressed: National Laboratory of Biomacromolecules, Institute of Biophysics, Chinese Academy of Sciences, 15 Datun Road, Beijing 100101, China. Tel: +86 10 64888490. Fax: +86 10 64872026. E-mail: jfw@sun5.ibp.ac.cn.

[1]Abbreviations: SNase, staphylococcal nuclease; CI-2, chymotrypsin inhibitor-2; CD, circular dichroism; pdTp, thymidine 3′,5′-bisphosphate; TMAO, trimethylamine *N*-oxide; HSQC, heteronuclear single-quantum correlation; NOE, nuclear Overhauser effect; NOESY, NOE spectroscopy; PDB, Protein Data Bank

 Published on Web 08/06/2009

types of complexes formed from SNase(1−126) and SNase-(50−149) were determined, and the factors involved in the formation of these complexes were analyzed (*15*). Of them, the complex of the fragments SNase(6−48) and SNase(49−149) has been crystallized in the presence of pdTp and Ca^{2+}. X-ray diffraction analysis of the crystals has shown that the structure of the complex closely resembles that of the crystal of nuclease in the presence of pdTp and Ca^{2+} (*16*). However, these studies did not report the nature of the interactions involved in the fragment recognition process and the mechanism of fragment complementation on the basis of complex structure.

Our previous studies have indicated that the N-terminal 1−110 residues fragment of SNase (SNase110) is largely unfolded. However, the G88W and V66W single mutations and the cosmotrophic effect of a small organic osmolyte TMAO (trimethylamine *N*-oxide) can make SNase110 to fold into a native-like β-subdomain conformation which comprises a "β-barrel" region and two helices α1 and α2 (*17*). Moreover, elongation of chain length of the SNase110 fragment from K110 up to E135 of the helix α3 in SNase can restore largely the nuclease activity and native-like fold (*18*). For ascertaining the role of the C-terminal small segment containing the helix α3 of SNase (named C-terminal α-subdomain) in stabilization of the N-terminal β-subdomain containing the "β-barrel" region and helices α1 and α2 of SNase, it is necessary to identify and characterize the interactions between two corresponding fragments.

In the present study, we have purified the N-terminal 1−121 residue fragment SNase121 and C-terminal 111−143 residue fragment SNase(111−143) and their mutant variants. Sequences of SNase121 and SNase(111−143) fragments correspond to that of the β- and α-subdomain of SNase, respectively. We have adopted an approach of fragment complementation to investigate the nature of the interactions between the two fragments. The SNase121:SNase(111−143) complex formation was verified by various biochemical and biophysical methods. The nuclease activities of the noncovalent complexes formed by the mutant N-terminal with the mutant C-terminal fragments were screened, and the solution structure of SNase121:SNase(111−143) complex was determined by multidimensional NMR spectroscopy. The mechanism of highly efficient structural complementation of SNase121 with SNase(111−143) having up to 30% of the nuclease activity was addressed.

MATERIALS AND METHODS

Protein Production. The N-terminal large fragments of SNase, namely, SNase121, SNase116, and SNase110 containing residues 1−121, 1−116, and 1−110, respectively, were expressed and purified according to the procedures described previously (*19*). The plasmids for SNase121 and SNase110 have been constructed in this lab. For constructing SNase116 plasmid, gene of SNase116 was cloned into a pET-3d expression vector with *Nco*I and *Bam*HI restriction enzyme sites.

Genetic construction, expression and purification of the C-terminal fragment SNase(111−143) containing residues 111−143 were described in the previous report (*20*). Gene manipulations for SNase(107−143) having extra residues 107−110 at the N-terminus of SNase(111−143), and for SNase(118−143), SNase-(119−143), and SNase(120−143) lacking the N-terminal residues 111−117, 111−118, and 111−119 of SNase(111−143), followed the protocols used for SNase(111−143). The plasmid constructions for N118G-, N119G-, T120A-, E122A-, R126L-, S128A-, E129A-, E135A-, N138G-, W140A-, W140F-, and S141A mutant SNase(111−143) fragments were achieved by site-directed mutagenesis of the gene of SNase(111−143).

Uniformly ^{15}N- and/or ^{13}C-labeled proteins were obtained by growth in M9 minimal media containing $^{15}NH_4Cl$ and/or [^{13}C]-glucose as the sole nitrogen and/or carbon sources, respectively. The purity of proteins was checked by SDS−PAGE to ensure a single band.

Nuclease Activity Assay. The enzyme activities for hydrolysis of single-stranded DNA were measured for full-length SNase, free SNase121, SNase121:SNase(111−143) complex, mixtures of SNase121 and mutant variants of SNase(111−143), and mixtures of various N-terminal large and C-terminal short SNase fragments with different chain lengths. The measurements were performed at 25 °C with a Shimadzu UV-250 spectrophotometer by monitoring the increase in absorbance at 260 nm. The single-strand salmon sperm DNA, obtained by boiling salmon sperm DNA at 100 °C for 30 min and rapidly cooled on ice, was used as a substrate of measurements. The activity assay was achieved according to the method described by Cautrecasas et al. (*21*).

Far-UV CD Measurement. Far-UV CD spectra (200−250 nm) were recorded on a Jasco 720 spectropolarimeter at 25 °C for full-length SNase, free SNase121 and SNase(111−143), and the mixture of SNase121 and SNase(111−143). Protein concentration was 0.4 mg/mL in 20 mM Tris-HCl buffer (pH 7.4). A quartz cuvette with 1.0 mm path length was employed in the measurements. Four scans were averaged for each measurement.

Fluorescence Measurements. The fluorescence emission spectra of residue W140 in the SNase(111−143) were used to monitor the conformational changes of SNase(111−143) upon addition of SNase121 in the sample. The tryptophan fluorescence titration spectra were recorded on a Hitachi F4500 fluorescence spectrophotometer at an excitation wavelength of 300 nm (slit width, 5 nm) and an emission wavelength of 300−400 nm (slit width, 5 nm). A circulating water bath was used to maintain the sample temperature at 298 K. The fluorescence titration experiments were performed by adding the increased amounts of SNase121 from a stock solution of 5.1 mg/mL (= 375.3 μM) protein in 20 mM Tris-HCl (pH 7.4) to a 1 mL SNase(111−143) sample containing 3 μM protein and 20 mM Tris-HCl (pH 7.4) in a 1 cm cell. Changes in fluorescence upon addition of the SNase121 stock solution were measured. The experimental data were fitted to the equation

$$F = F_{\min} + \left(\frac{[A_{\text{tot}}] + [B_{\text{tot}}] + K_{\text{d}}}{2} - \sqrt{\frac{([A_{\text{tot}}] + [B_{\text{tot}}] + K_{\text{d}})^2}{4} - [A_{\text{tot}}][B_{\text{tot}}]} \right) \frac{(F_{\max} - F_{\min})}{[A_{\text{tot}}]} \quad (1)$$

where $[A_{\text{tot}}]$ is the SNase(111−143) concentration, $[B_{\text{tot}}]$ is the total SNase121 concentration for each measurement, F is the measured fluorescence intensity of the complex at the desired SNase121 concentration, and $F_{\max}$ and $F_{\min}$ are the maximal and minimal fluorescence intensity of the complex, respectively. Nonlinear regression curve fitting was carried out for fitting the experimental data to the equation with $F_{\max}$, $F_{\min}$ and K_{d} as fitted parameters (*22*, *23*). Since the total volume of SNase121 (25 μL) added in the solution is much smaller than the sample

volume (1 mL), the change in protein concentration as a result of SNase121 addition was very small and can be ignored.

Size-Exclusion Chromatography. Size-exclusion chromatography was used to elute the mixture of SNase121 and SNase(111−143) and mixture of SNase110 and SNase(111−143) in 1:1 stoichiometric ratio as well as free SNase121, SNase110, SNase(111−143), and native SNase. The protein concentration was 1.0 mM. Gel filtration chromatography was carried out on a Bio-Sil HPLC size exclusion column (Bio-Rad), equilibrated with gel filtration buffer (20 mM Tris-HCl buffer, pH 7.0, 100 mM KCl). Samples were prepared by dissolving proteins in buffer (50 mM Tris-HCl, 100 mM KCl, pH 7.0), and were eluted with the sample buffer. The column was run at 4 °C with a flow rate of 1.0 mL/min. The effluent of each sample was monitored by measuring absorbance at 280 nm.

NMR Titration Experiments. In order to characterize the binding features of SNase121 and SNase(111−143) during the formation of their native-like conformations in the complex, titration of SNase121 with SNase(111−143) and reverse titration were monitored by 2D $^{1}H-^{15}N$ HSQC spectra of titrated SNase121 and SNase(111−143). The 2D $^{1}H-^{15}N$ HSQC spectra of 0.5 mM ^{15}N-labeled SNase121 were acquired at 0.1, 0.2, 0.3, 0.4, 0.5, 0.6, 0.7, 0.8, and 1.0 mM unlabeled SNase(111−143). In the reverse titration experiments, the concentration of SNase(111−143) was fixed at 0.5 mM, and 2D $^{1}H-^{15}N$ HSQC spectra of SNase(111−143) were recorded at the increased amounts (0.1, 0.2, 0.3, 0.4, 0.5, 0.6, 0.7, 0.9, 1.1 mM) of unlabeled SNase121.

NMR Spectroscopy. The SNase fragments and fragment mixtures used in the corresponding experiments were dissolved in aqueous solution containing 50 mM deuterated acetate buffer (pH 5.0), 100 mM KCl, and 0.01% (w/v) NaN_3. Mixtures of the N- and C-terminal SNase fragments were composed of 1.0 mM isotope-labeled N-terminal SNase fragments and unlabeled C-terminal SNase fragments in 1:1 stoichiometric ratio or *vice versa*. The SNase121:SNase(111−143) complexes were prepared by mixing 1.0 mM isotope-labeled SNase121 or SNase(111−143) with 5% excess unlabeled SNase(111−143) or SNase121, respectively.

All NMR experiments were run on a Bruker DMX 600 spectrometer equipped with a triple-resonance cryo-probe at 300 K. The 3D $^{1}H-^{13}C-^{15}N$ HNCACB, CBCA(CO)NH, C-(CO)NH-TOCSY, HN(CA)CO, HNCO, H(CCO)NH-TOCSY, and the 3D $^{1}H-^{15}N$ and $^{1}H-^{13}C$ TOCSY-HSQC (τ_m = 60 ms) and NOESY-HSQC (τ_m = 130 ms) experiments were performed for assignments of backbone and side-chain ^{1}H, ^{15}N, and ^{13}C resonances and intramolecular NOE connectivities in the complex. The binding surface of SNase121:SNase(111−143) complex was detected in H_2O using modified 4D ^{13}C,^{1}H-HMQC-NOESY-^{15}N,^{1}H-HSQC experiment at mixing time of 150 ms, and the intermolecular NOEs were detected in D_2O using 3D ω_1-filter-NOESY-^{13}C,^{1}H-HSQC experiment at mixing time of 130 ms (*24*).

Backbone ^{15}N T_1 and T_2 and $^{1}H-^{15}N$ NOE relaxation parameters were measured for SNase121:SNase(111−143) complex as well as native SNase using standard experiments (*25*, *26*). For SNase121:SNase(111−143) complex, T_1 relaxation decay was sampled at time points of 10, 30, 80, 160, 280, 380, 530, 760, 1200, and 1600 ms, T_2 decay was sampled at time points of 8.48, 16.96, 25.44, 33.92, 50.88, 67.84, 84.8, 101.76, 118.72, 135.68, and 152.64 ms, T_1 and T_2 measurements used a recycle delay of 2.5 s, and NOE measurements used a delay time of 7 s followed by a ^{1}H saturation of 3 s. For native SNase, the relaxation measurements were performed using a similar experimental setup, except the T_1 measurements which were performed using the delay times of 20, 62, 142, 282, 382, 522, 822, 1202, and 1602 ms. Analyses of ^{15}N relaxation data and parameters of backbone internal motions were performed following the methods described previously (*27*, *28*). The R_2/R_1 ratios of a set of residues selected by excluding residues with very high R_2 and low NOE values (< 0.7) were used to determine the rotational diffusion tensors that describe the overall tumbling. Optimization of the rotational diffusion and the model-free parameters against the experimental data was performed using TENSOR version 2.0 (*29*). Model selection is based on extensive *F*-statistical testing and implemented in TENSOR version 2.0 (*30*−*32*).

All NMR data were processed and analyzed using FELIX98 (Accelrys Inc.). The data points in each indirect dimension were usually doubled by linear prediction before zero filling to the appropriate size. 90° to 60° shifted square sine bell apodizations were used for all three dimensions prior to Fourier transformation.

Structure Calculation. All assigned intramolecular NOEs were grouped into five classes of distance restraints: 1.8−2.5 Å, 1.8−3.5 Å, 1.8−4.5 Å, 1.8−5.5 Å, and 1.8−6.0 Å. All intermolecular NOEs were grouped into 1.8−5.5 Å and 1.8−6.0 Å distance restraints. Intramolecular backbone hydrogen bond restraints were generated from the secondary structural elements of the complex based on the backbone chemical shift data and NOE patterns (short HN−O distances). The hydrogen bond restrictions were applied very loosely: the distance restraints of O···H and O···N in hydrogen bond were set to 2.0 ± 0.5 Å and 3.0 ± 0.5 Å. Backbone torsion angle restraints were obtained using the program TALOS (*33*) and imposed only for those residues that exhibited TALOS reliability scores of 10. The solution structures of SNase121:SNase(111−143) complex were calculated with the program CNS 1.2 (*34*). A family of 200 structures was generated, and 50 structures with lowest energies were selected and refined in explicit water (*35*) using RECOORD-Script (*36*), from which a final set of the 20 structures with lowest energies was considered for use in the analysis of structural statistics. Structural analysis and statistics were obtained using programs MOLMOL (*37*) and PROCHECK-NMR (*38*).

RESULTS

Nuclease Activities of Mixtures of the SNase Fragments. The functional complementation of the SNase fragments was assessed by measuring the nuclease activity. The nuclease activity was measured for mixtures of the N-terminal large fragments (SNase121, SNase116, and SNase110) with the C-terminal small fragments, namely, SNase(107−143), SNase(111−143), SNase(118−143), SNase(119−143), and SNase(120−143), and for SNase121 with various mutants of SNase(111−143) (Table 1). The free SNase121 showed 7% of the nuclease activity of the native level since the DNA binding can induce the folding of SNase121 during the nuclease activity assay. However, the nuclease activity of SNase121 mixed with SNase(111−143) was resumed up to 30% of the activity of the native level. All other mixtures showed lower nuclease activities compared to the mixture of SNase121 and SNase(111−143). The mixtures of SNase121 with SNase(118−143), SNase(119−143), and SNase(120−143) can restore only 19%, 9%, and 6% nuclease activities to SNase121, respectively. These revealed that residues preceding N119 of SNase(111−143) are required for restoring the nuclease

Table 1: Relative Nuclease Activities of Mixtures of Various N- and C-Terminal SNase Fragments to the Activity of SNase[a]

SNase fragment mixture	rel act. (%)
SNase121 + SNase(111−143)	30
SNase121 + SNase(118−143)	19
SNase121 + SNase(119−143)	9
SNase121 + SNase(120−143)	6
SNase116 + SNase(111−143)	5.5
SNase116 + SNase(118−143)	3.5
SNase110 + SNase(107−143)	3
SNase110 + SNase(111−143)	2
SNase121	7
SNase121 + [N138G]SNase(111−143)	24
SNase121 + [S128A]SNase(111−143)	23
SNase121 + [S141A]SNase(111−143)	18
SNase121 + [T120A]SNase(111−143)	17
SNase121 + [E135A]SNase(111−143)	13
SNase121 + [N118G]SNase(111−143)	12
SNase121 + [N119G]SNase(111−143)	12
SNase121 + [E122A]SNase(111−143)	10
SNase121 + [R126L]SNase(111−143)	10
SNase121 + [E129A]SNase(111−143)	9
SNase121 + [W140F]SNase(111−143)	9
SNase121 + [W140A]SNase(111−143)	6

[a]The enzyme activity of SNase121 is listed for comparison.

activity of the SNase121 and SNase(111−143) mixture, especially, residues P117−N119 of SNase(111−143) played an important role in resuming up a higher nuclease activity of SNase121 in the mixture. SNase110 in mixture with SNase(111−143) or even with SNase(107−143) showed only 2−3% of native nuclease activity. However, SNase116 in mixture with SNase(111−143) or even with SNase(118−143) can yield 5.5% and 3.5% of native nuclease activity, respectively. This implies that residues V111−K116 of SNase121 are important for restoration of the active site in the mixture with the C-terminal fragments. Moreover, some mutations of SNase(111−143) reduced largely the nuclease activity of the SNase121 and SNase(111−143) mixture. Therefore, SNase121 can associate with SNase(111−143) in the mixture through noncovalent interactions, forming a most native-like active site for degrading both DNA and RNA among all other mixtures, and these noncovalent interactions may be disturbed by amino acid replacement in the sequence of SNase(111−143).

Complementation of the N- and C-Terminal SNase Fragments in the Mixture. Complementation of the N- and C-terminal SNase fragments in the mixture can be detected using 2D $^{1}H-^{15}N$ HSQC spectra of the corresponding fragments in the mixture. Figure 1 shows the 2D $^{1}H-^{15}N$ HSQC spectra of two SNase fragments, SNase121 and SNase(111−143), in the free state and in the mixture. The free SNase121 was in the largely unfolded state which was in exchange with partially folded states (*18*), whereas free SNase(111−143) has nonordered conformation in aqueous solution (*20*). The 2D $^{1}H-^{15}N$ HSQC spectrum of ^{15}N-labeled SNase121 in mixture with unlabeled SNase(111−143) showed the cross peaks of amide resonances distributed in the whole spectral region (Figure 1A), whereas the cross peaks of free SNase121 crowded a narrow range of 7.8−8.8 ppm of $^{1}H_N$ resonances in the spectrum (Figure 1B). This revealed that SNase121 in the mixture likely adopted a native-like β-subdomain conformation of SNase, as many of the unique dispersed cross peaks observed for resonances in the spectrum of native SNase (Figure 1C) or in the spectrum of folded G88W mutant SNase121 (G88W121) (Figure 1F) are recovered in the spectrum of SNase121 in the mixture (Figure 1A). The ^{15}N-labeled SNase(111−143) in mixture with unlabeled SNase121 showed dispersed cross peaks in the spectrum (Figure 1D), representing a folded conformation. However, the amide proton resonances for free SNase(111−143) showed little chemical shift dispersion (Figure 1E), indicating a largely unfolded conformation of the fragment. Therefore, SNase121 can structurally complement with SNase(111−143).

SNase110 in the mixture with SNase(111−143) provided a 2D $^{1}H-^{15}N$ HSQC spectrum identical to the spectrum obtained for free SNase110, revealing that SNase(111−143) has no capability to associate with SNase110 (Figure 1A,B in the Supporting Information). SNase116 upon mixing with SNase(111−143) generated a spectrum showing broad resonances in the center of the spectrum (Figure 1C in the Supporting Information), which indicated the presence of a small amount of unfolded protein in the sample. Similar to the mixture of SNase116 and SNase(111−143), SNase121 mixed with SNase(118−143), SNase(119−143), and SNase(120−143) provided spectra with increased number of broad resonances squeezed in the center of the spectrum of SNase121 (Figure 1D−F in the Supporting Information), indicating a certain amount of unfolded SNase121 in these mixtures. Therefore, residues V111−K116 and P117−N119 are the essential C- and N-terminal segments for N-terminal β-subdomain and C-terminal α-subdomain fragments of SNase, respectively, to have a high efficiency of the complementation in the mixture. The best complementation was obtained with the fragments SNase121 and SNase(111−143).

The SNase121:SNase(111−143) Complex Has a Native-like Conformation. To detect whether a SNase121:SNase(111−143) noncovalent complex is formed, the size-exclusion experiment was performed with a sample of an equal molar ratio of SNase121/SNase(111−143). The size-exclusion chromatograms were also taken for free SNase121 and SNase(111−143) as well as native SNase. The chromatogram of SNase121 and SNase(111−143) mixture showed a major peak with a retention time of ∼16.4 min and a weak minor peak at ∼14.3 min, which is almost identical to the chromatogram of native SNase (Figure 2). This means the mixture was eluted from the gel filtration column as a single protein species. Due to a larger size of structureless SNase(111−143) in solution despite its smaller molecular weight, the free SNase(111−143) eluted at ∼14.1 min much earlier than both the native SNase and the mixture of SNase121 and SNase(111−143), whereas free SNase121 eluted at 15.9 min (Figure 2). Thus, SNase121 and SNase(111−143) can form a complex having a folded conformation similar to that of native SNase. However, the chromatogram of SNase110 and SNase(111−143) mixture was largely different from those of SNase121:SNase(111−143) complex and native SNase (Figure 2 in the Supporting Information), indicating that noncovalent complex was not formed in the SNase110 and SNase(111−143) mixture.

The CD spectrum of the SNase121:SNase(111−143) complex is largely different from the spectra of free SNase121 and SNase(111−143), showing two negative minima at about 208 and 222 nm. The overall shape of the complex spectrum resembles the spectrum of native SNase (Figure 3 in the Supporting Information). The fluorescence measurements indicated that association of fragments SNase121 and SNase(111−143) leads to a shift in the fluorescence emission spectrum with a maximum at 336 nm, resembling the emission spectrum of native SNase. Moreover, the relative molar intensity

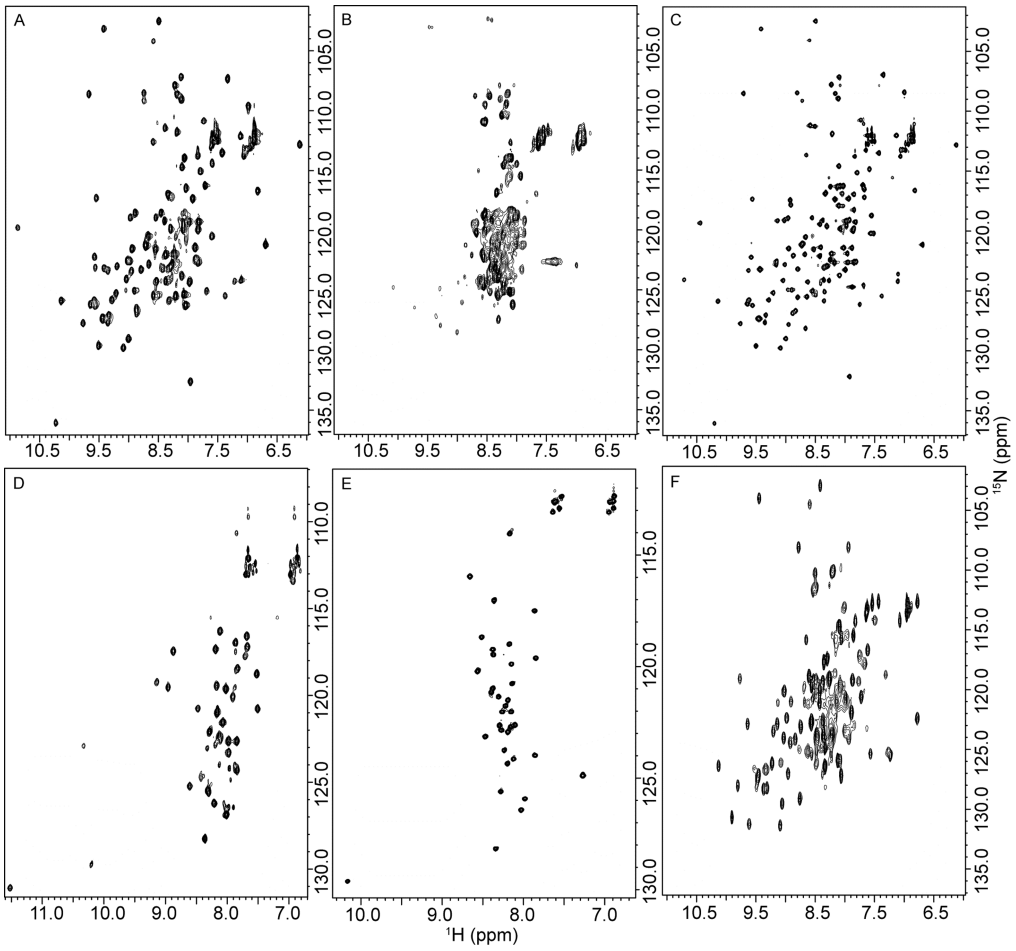

FIGURE 1: 2D $^{1}H-^{15}N$ HSQC spectra of free SNase121 and SNase(111−143) and the mixture of two fragments. The spectra of native SNase and G88W mutant SNase121 (G88W121) are given for comparative analysis. (A) ^{15}N-Labeled SNase121 mixed with unlabeled SNase(111−143). (B) Free SNase121. (C) Full-length SNase. (D) ^{15}N-Labeled SNase(111−143) mixed with unlabeled SNase121. (E) Free SNase(111−143). (F) G88W121.

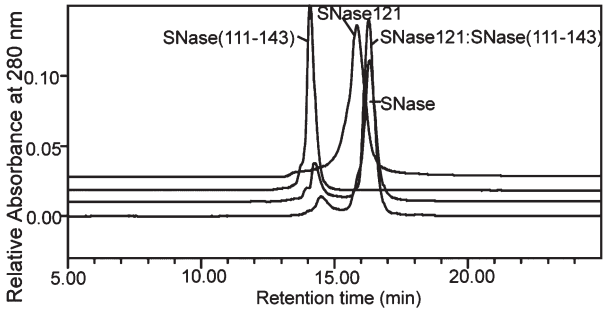

FIGURE 2: Elution profiles of an equal molar mixture of SNase121 and SNase(111−143) from size-exclusion chromatography. For comparison, the chromatograms of free SNase121 and SNase-(111−143) as well as SNase are provided.

of the emission of the complex at 336 nm reached up to approximately 27.6% of native SNase at 336 nm (Figure 4A in the Supporting Information). These evidenced again that the SNase121 and SNase(111−143) fragments can form a noncovalent complex having a native-like conformation upon association.

Binding Features of SNase121 and SNase(111−143) in the Complex. To elucidate how the binding of SNase121 and SNase(111−143) to each other induces SNase121 and SNase-(111−143) resuming their native conformations, namely, the β- and α-subdomain conformations of SNase, respectively, a series of 2D $^{1}H-^{15}N$ HSQC spectra of ^{15}N-labeled SNase121 and SNase(111−143) were recorded in the presence of increased amounts of unlabeled SNase(111−143) and SNase121, respectively. Interestingly, in the titration of ^{15}N-labeled SNase121 with unlabeled SNase(111−143), the 2D $^{1}H-^{15}N$ HSQC spectra of SNase121 did not show any shift of resonance signals as the concentration of SNase(111−143) was increased (Figure 3). Upon addition of 0.1 mM SNase(111−143), some cross peaks in the narrow spectral region (7.8−8.8 ppm) of $^{1}H_{N}$ resonances decreased in intensity and new cross peaks appeared at different dispersed positions in the 2D HSQC spectrum of SNase121. Apparently, the newly appeared cross peaks should belong to the SNase(111−143)-bound state of SNase121. During the titration, these cross peaks did not show any shifting, and their intensities were increased with increasing of SNase(111−143) concentrations and reached constant at a SNase(111−143)/SNase121 ratio above 1.

In the titration of ^{15}N-labeled SNase(111−143) with unlabeled SNase121, the 2D $^{1}H-^{15}N$ HSQC spectrum of SNase(111−143) at 0.1 mM SNase121 is very similar to those of unfolded SNase(111−143) (Figure 5A in the Supporting Information, and Figure 1E). Upon addition of 0.2 mM SNase121, the weak resonance signals for SNase(111−143) appeared in the spectrum, which showed a dispersion pattern similar to the signal displacement in the 2D HSQC spectrum of SNase(111−143) in the

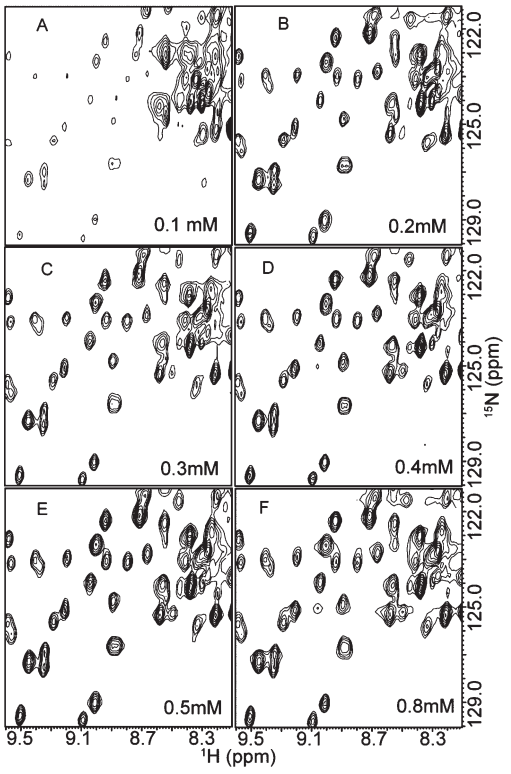

FIGURE 3: Titration of ^{15}N-labeled SNase121 with unlabeled SNase(111−143). The 2D ^{1}H−^{15}N HSQC spectra of 0.5 mM SNase121 were acquired by titration with SNase(111−143) of increased concentrations: 0.1 (A), 0.2 (B), 0.3 (C), 0.4 (D), 0.5 (E), and 0.8 (F) mM.

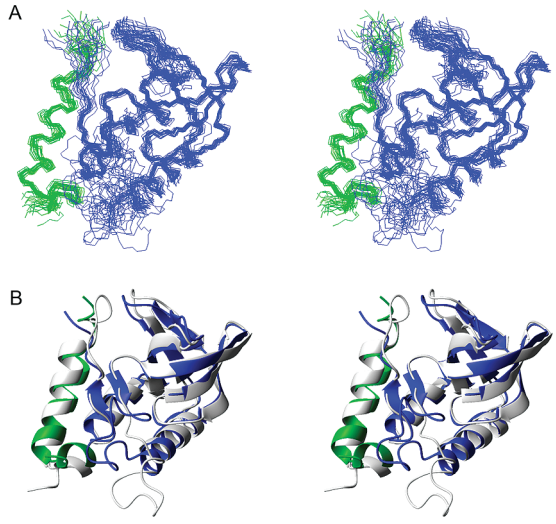

FIGURE 4: The stereoview of the solution structure of SNase121:SNase(111−143) complex. (A) Superposition of the 20 lowest energy conformers calculated for the complex. The backbone of SNase121 is shown in blue, those of SNase(111−143) in green. (B) Ribbon structure of a representative conformer of the complex (SNase121 in blue and SNase(111−143) in green) superimposed to structure of native SNase (silver gray). The residues 1−6 and 117−121 of SNase121 and the residues 111−116 of SNase(111−143) in the complex, and the residues 1−6 and 144−149 of native SNase as well, are not shown. In panel B, the loops showing different conformations in the blue vs silver gray structure are the pdTp-binding loop and the Ω-loop.

complex (Figure 5B in the Supporting Information, and Figure 1D). Clearly, the resonance signals for both SNase(111−143) in the free unfolded state and in the SNase121-bound state showed up in the titration spectra. With the increase of SNase121 concentrations, the intensities of signals from SNase(111−143) in the SNase121-bound state were increasing whereas those from the free unfolded SNase(111−143) were decreasing (Figure 5C−F in the Supporting Information).

The above observed phenomenon that the newly appeared dispersed cross peaks showed no shifting in the titration spectra indicated that SNase121 and SNase(111−143) in the free and bound states were in slow exchange at the NMR time scale, which suggested a tight binding between them. The fluorescence titrations were carried out to estimate the dissociation constant (K_d) between SNase121 and SNase(111−143) (Figure 4B in the Supporting Information) (*22*, *23*). The obtained K_d value of the SNase121:SNase(111−143) complex is about 0.36 ± 0.09 μM. Therefore, fragments SNase121 and SNase(111−143) associate tightly to form a stable noncovalent complex.

Solution Structure of the SNase121:SNase(111−143) Complex. Assignments of ^{1}H, ^{13}C, and ^{15}N resonances and intramolecular NOEs of SNase121 and SNase(111−143) in the complex and intermolecular NOEs between SNase121 and SNase(111−143) have been identified. Figure 6 in the Supporting Information shows the assignments of amide resonances for SNase121 and SNase(111−143) in the complex. Intermolecular NOEs between side chains of the residues at the binding interface were detected for the complex samples containing ^{13}C-labeled SNase121 and unlabeled SNase(111−143) and *vice versa* (Table 1 in the Supporting Information). The main-chain to main-chain and main-chain to side-chain intermolecular NOEs between residues involved in the binding interface were also obtained unambiguously by manual assignments using ^{1}H−^{15}N NOESY-HSQC spectra (Table 2 in the Supporting Information).

The solution structure of the SNase121:SNase(111−143) complex was calculated using the intramolecular and intermolecular NOE-derived restraints in combination with the intramolecular dihedral angle and hydrogen bond restraints. Figure 4A shows the superposition of the 20 lowest energy SNase121:SNase(111−143) complexes. PROCHECK-NMR analysis (*39*) showed a good backbone conformational regularity for 80.4% of all residues in the most favored regions. Detailed structural statistics and analysis of the ensemble of SNase121:SNase(111−143) complex are summarized in Table 2. The overall structure of the SNase121:SNase(111−143) complex is essentially the same as those of full-length SNase (PDB code: 1JOO) except the loop of residues V111−H121 of SNase. The solution structure of SNase121 in the complex has a conformation almost identical to the conformation of the β-subdomain of SNase except the C-terminal region of residues K116−H121 in the fragment SNase121. The structure of SNase(111−143) in the complex contains an α-helix of residues E122−K136 with a C-terminal loop of residues L137−D143, which is very similar to the conformation of the α-subdomain of native SNase except the N-terminal region of residues V111−Y115 in the fragment SNase(111−143) (Figure 4B). Therefore, the SNase121 and SNase(111−143) fragments have the folded native-like β-subdomain and α-subdomain structures of SNase, respectively, in the complex, and the SNase121:SNase(111−143) complex structure is essentially the same as the tertiary structure of native SNase.

Binding Surfaces between SNase121 and SNase(111−143). The interactions between SNase121 and SNase(111−143) in the complex are mediated by the surface residues in both fragments. Residues constituting the binding interface

between SNase121 and SNase(111−143) were determined by heteronuclear NMR experiments. The cross peaks shown in Figures 7A and 7B in the Supporting Information correspond to the surface residues of SNase121 and SNase(111−143) in the complex, respectively (Figure 7C in the Supporting Information). The close contacting residues at the interface between SNase121 and SNase(111−143) were also identified using distance cutoff <5.5 Å (Tables 1 and 2 in the Supporting Information). Mapping of these residues to the structure of SNase121:SNase(111−143) complex (Figure 5A) suggested that the interaction surface comprised three regions. The first is mainly composed of residues Y115−T120 in the N-terminal region of SNase(111−143) and the portions (residues D77−Q80) of the pdTp-binding loop (p-loop, D77−L89) as well as residues in the segment V111−K116 of SNase121. The second consists of the helix α3 (E122−K136) in SNase(111−143) and the helix α2 (V99−Q106) and the short strand β8 (A109−V111) as well as L38 and A112 in SNase121 (Figure 5A,B). The third is between the segment (residues Q106−A109) linking the helix α2 and the strand β8 in SNase121 and the C-terminal loop of L137−E142 in SNase(111−143) (Figure 5A,C).

Table 2: NMR-Derived Geometrical Restraints and Structural Statistics for the Family of 20 Structures of SNase121:SNase(111−143) Complex

	SNase121	SNase (111−143)	complex
NMR Structural Restraints			
intraresidue NOEs ($\|i-j\|=0$)	887	319	
sequential NOEs ($\|i-j\|=1$)	494	167	
medium-range NOEs ($\|i-j\|=2-4$)	152	96	
long-range NOEs ($\|i-j\|>4$)	427	23	
total NOEs	1960	605	
intermolecular NOEs			71
hydrogen bond restraints	42	15	
dihedral angle restraints: ϕ, ψ each	76, 77	16, 16	
No. of Restraint Violations (Maximal Violation)			
distance restraint >0.3 Å	0 (0.273 Å)		
dihedral >5°	0 (4.94°)		
Ramachandram Analysis (% Residues)			
most favored regions	80.4%		
additional allowed regions	15.7%		
generously allowed regions	1.7%		
disallowed regions	2.1%		
Average Rms Deviations from the Mean[a]:			
backbone heavy-atoms (Å)	0.59 ± 0.11		
All heavy atoms (Å)	1.12 ± 0.12		

[a] For secondary structure region: 8−11, 13−17, 22−26, 31−35, 39−41, 58−69, 72−76, 90−93, 99−106, 109−111, 122−136.

In the three surface regions, the residues involved in the main-chain and side-chain contact interactions are as follows. In the first region, residues K78 and G79 in the p-loop of SNase121 are placed closely to residues N118 and T120 in the N-terminal loop of SNase(111−143). In addition, residue N118 of SNase(111−143) is close to residues V114, Y115, and K116 of SNase121 (Figure 5A, and Tables 1 and 2 in the Supporting Information). For the second region, residues E101, V104, R105, and Q106 in the helix α2 and V111 in the strand β8 of SNase121 have close contacts with residues L125, R126, S128, and E129 in the helix α3 of SNase(111−143). According to the complex structure and the close contacts of L125 with L38 and V111, the hydrophobic side chain of L125 of SNase(111−143) points into a hydrophobic cluster which is composed of L38, V104, V111, and A112 of SNase121 in this region (Figure 5B, and Tables 1 and 2 in the Supporting Information). Residues G107, L108, and A109 of SNase121 and A132, L137, N138, I139, and W140 of SNase(111−143) have close contacts in the third region. The pyrrole ring of W140 is surrounded by the hydrophobic side chains of G107, L108, A109, A132, L137, and I139 and the long hydrophobic side chains (Cβ−ζ) of amphiphilic residues K110 and K133 in the complex structure (Figure 5C, and Tables 1 and 2 in the Supporting Information).

Backbone Dynamics of SNase121:SNase(111−143) Complex. In order to characterize the internal motions of SNase121:SNase(111−143) complex, the R_1 and R_2 relaxation rates and $^1H-^{15}N$ NOEs were determined for both ^{15}N-labeled SNase121 and SNase(111−143) in the complex. The relaxation parameters R_1, R_2, and $^1H-^{15}N$ NOEs of SNase121:SNase(111−143)

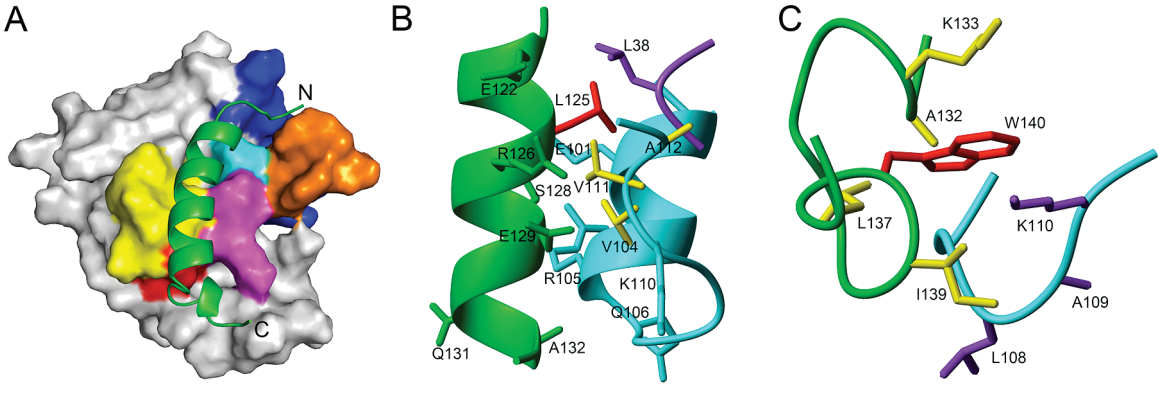

FIGURE 5: Representation of binding surface in the SNase121:SNase(111−143) complex. (A) Surface representation of the binding regions mapped to SNase121 in the complex. Residues in the p-loop are colored blue, residues Y113−K116 are colored orange, magenta color indicates the residues in the strand β8, and yellow color indicates the residues in the helix α2. The linker between the helix α2 and the strand β8 is colored red. Residues L38 and A112 are colored cyan. Backbone of SNase(111−143) is represented by a green ribbon. (B) View on the second binding region of SNase(111−143) to SNase121 in the complex. Backbones are represented by ribbon, and amino acid residues are shown with their side chain. In SNase121, backbone of the strand β8 and the helix α2 and hydrophilic residues are colored in cyan, and hydrophobic residues in yellow. Residue L38 is in purple. SNase(111−143) backbone and residues are colored in green. Residue L125 is highlighted in red. (C) View on the region including the segment linking the helix α2 and the strand β8 (cyan) in SNase121 and the C-terminal loop of L137−E142 (green) in SNase(111−143). Residue W140 is highlighted in red.

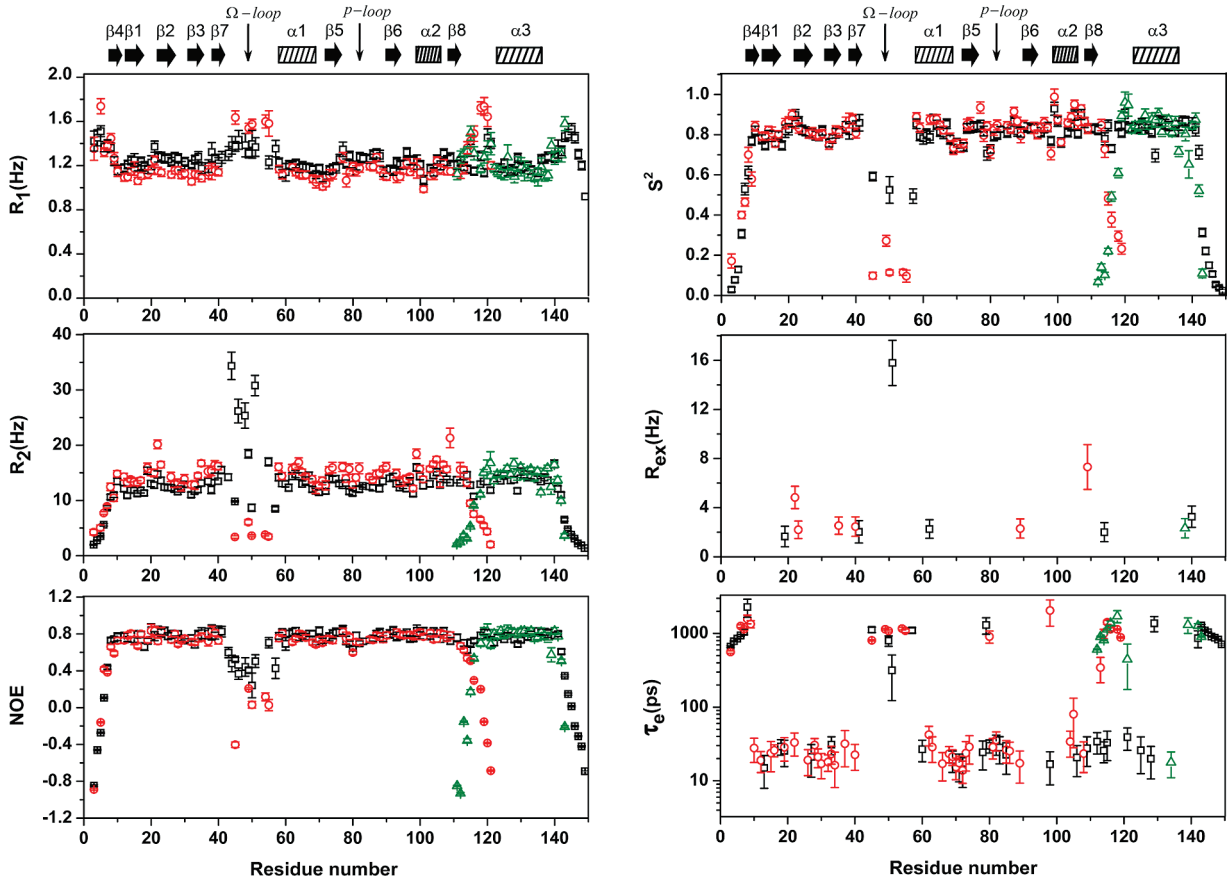

FIGURE 6: Sequence variation of ^{15}N relaxation parameters and model-free parameters of SNase121:SNase(111−143) complex. Data for ^{15}N-labeled SNase121 in the complex with unlabeled SNase(111−143) are colored in red. Data for ^{15}N-labeled SNase(111−143) in the complex with unlabeled SNase121 are colored in green. The relaxation parameters of SNase are provided (black) for comparison. Positions of the secondary structures are marked at the top of the diagrams.

complex are given in Figure 6. Sequence variations of these relaxation parameters were observed for the Ω-loop (P42−P56) and both N- and C-terminal regions of fragment SNase121, and also for the N- and C-terminal segments of fragment SNase(111−143) in the complex. The N- and C-terminal regions of residues preceding residue E10 and following residue Y113, respectively, in SNase121 and of residues preceding P117 and following residue S141, respectively, in SNase(111−143) were flexible with ^{1}H−^{15}N NOE values <0.6. In the Ω-loop, several detectable residues of SNase121 showed the ^{1}H−^{15}N NOE values <0.4. The ordinary secondary structural elements and the p-loop in SNase121 and the helix α_3 in SNase(111−143) have higher ^{1}H−^{15}N NOE values (>0.7), reflecting the highly restricted high-frequency motions of these regions. The R_1 and R_2 rates for SNase121 and SNase(111−143) in the complex were fairly constant within the regular secondary structural regions, having the average values of 1.12 ± 0.04 and 14.79 ± 0.71, respectively, for SNase121 and 1.13 ± 0.06 and 14.79 ± 0.58, respectively, for SNase(111−143). However, similar to both terminal regions in SNase121 and SNase(111−143), the residues in Ω-loop have higher than the average values of R_1 but lower than the average value of R_2. This indicated that the backbone of secondary structural regions in SNase121 exhibited low internal mobility whereas those of Ω-loop was less ordered and exhibited large amplitude motion on the sub-nanosecond time scale.

The relaxation parameters of SNase121:SNase(111−143) complex were analyzed by the Lipari−Szabo model-free formalism (*40*, *41*). The determined correlation time for overall rotational motion (τ_m) and axially symmetric diffusion tensor components and the angles (θ and φ) for SNase121:SNase(111−143) complex are listed in Table 3. Figure 6 shows the obtained model-free parameters S^2, τ_e, and R_{ex}. Examination of the general order parameters (S^2) indicated that residues in the sequence regions E10−D40 and A58−V114 of SNase121 and N119−E141 of SNase(111−143) in the complex have an average S^2 value of 0.84 ± 0.03. This implies that the backbone of the secondary structural regions in the complex exhibits restricted internal mobility. However, the Ω-loop of SNase121 in the complex is highly flexible with low motional restriction, as reflected by the fact that some contiguous residues in this loop have S^2 values well below 0.4 and τ_e times in the range 800−1200 ps. Both flexible terminal regions of SNase121 and SNase(111−143) in the complex have gradually decreased S^2 values and τ_e times exceeding 500 ps.

Table 3: Global Tumbling Dynamic Parameters Optimized from Model-Free Analysis

	SNase	SNase121:SNase(111−143)
τm (ns)	9.91 ± 0.029	11.14 ± 0.036
$D_{\parallel}/D_{\perp}$	1.31 ± 0.019	1.17 ± 0.018
θ (deg)	24.77 ± 1.97	-104.84 ± 3.95
φ (deg)	175.24 ± 4.90	135.91 ± 4.86

The relaxation data of SNase121 and SNase(111−143) in the complex clearly demonstrated that the backbone internal motions of the complex were very similar to that of native SNase,

except the Ω-loop of SNase121 and C- and N-terminal regions of SNase121 and SNase(111−143), respectively (Figure 6). This indicated that the stability of folded SNase121 and SNase(111−143) fragments in the complex is similar to that of the corresponding structural regions in native SNase. Therefore, the final rigid structure of each of SNase121 and SNase(111−143) fragments in the complex forms simultaneously with complex stabilization. It is likely that the native-like backbone mobility plays a role in structural adaptability at the binding interface of the two fragments in the recognition process.

DISCUSSION

Crucial Elements for Structural Complementation of the Two Fragments. The largely unfolded SNase121 and structureless SNase(111−143) can recognize each other and recover their native conformations upon mixing, restoring the active site and the ability to degrade DNA. This indicates that each fragment is strongly influenced by the presence of the other, and some interfering communications must occur through the recognition elements of SNase121 and SNase(111−143). The important elements for recognition and complementation of the two fragments should be identified in the three regions of the binding interface in the SNase121:SNase(111−143) complex.

(*a*) *V111−K116 of SNase121 and P117−N119 of SNase(111−143) Are the Two Segments Essential for Functional Complementation*. In the structure of native SNase, a loop of residues A112−H121 links the short strand β8 (A109−V111) of the N-terminal β-subdomain and the helix α3 (E122−K136) of the C-terminal α-subdomain of the protein, which forms a DNA binding cleft with the p-loop (*42*). Within a turn of residues Y115−N118 around the X-prolyl bond K116−P117 in the A112−H121 loop, the close contacts (using the distance cutoff of 5.5 Å) were identified between the backbone heavy atoms of residues Y115−P117, K116−N118, and Y115−N118 (*42*, *43*). It would appear from the structural information of native SNase that residues in the A112−H121 loop should be shared between fragments SNase121 and SNase(111−143) in the noncovalent complex. Thus, the complementary N-terminal large and C-terminal small SNase fragments must contain A112−K116 and P117−H121 sequences, respectively, in order to reactivate the complex. This implies that these residues, or their near-neighbors, or both, must be held firmly in the two fragments in order to form an essential part of the active site in the complex structure.

For the SNase121:SNase(111−143) complex, the close contacts of residue N118 of SNase(111−143) with residues V114, Y115, and K116 of SNase121 were obtained (Table 2 in the Supporting Information). Besides, the nuclease activity of the complex can be resumed up to 30% of the activity of the native level. It means segments A112−K116 and P117−H121 of SNase121 and SNase(111−143), respectively, together can be a mimic A112−H121 loop in the complex, and thus can restore the binding cleft with the p-loop of SNase121 for more efficiently degrading DNA. As revealed by measuring the nuclease activity and by the NMR experiments, SNase110 containing no residues V111−K116 in the sequence showed only residual nuclease activity while mixed up with SNase(111−143). SNase(119−143) and SNase(120−143) shortening residues P117−N118 and P117-N118-N119 at the N-terminal, respectively, in the complex with SNase121 can yield the nuclease activity only at the level of the free SNase121. Therefore, residues V111−K116 and P117−N119 are the two essential recognition segments of SNase121 and SNase(111−143), respectively, for functional complementation of these two SNase fragments.

(*b*) *Residue W140 Is Crucial for Highly Efficient Complementation of SNase(111−143) to SNase121*. Residue W140 is surrounded by the hydrophobic residues G107, L108, A109, A132, L137, and I139 as well as two amphiphilic residues K110 and K133 in the native SNase. In the SNase121:SNase(111−143) complex, W140 is placed in the similar hydrophobic environment which, however, is formed by G107, L108, A109, and K110 from SNase121 and A132, K133, L137, and I139 from SNase(111−143) (Figure 5C). For clarifying the role of W140 in the recognition process of the two fragments, residue W140 was mutated in SNase(111−143). Indeed, the recognition process of SNase(111−143) with SNase121 was influenced by mutation of tryptophan at sequence position 140 of SNase(111−143). The W140A mutant SNase(111−143) ([W140A]SNase(111−143)) in mixture with SNase121 can restore only 6% nuclease activities (Table 1), and the 2D $^{1}H-^{15}N$ HSQC spectrum of SNase121 in the mixture with [W140A]SNase(111−143) is very similar to the spectrum of the free SNase121 (Figure 8A,B in the Supporting Information), showing two sets of cross peaks for residues G29, K70, and D95 in the 2D HSQC spectrum. As was reported, the conformational heterogeneity of SNase121 in solution was represented by two sets of cross peaks for residues G29, K70, and D95 in the 2D HSQC spectrum which is linked with the prolyl *cis*−*trans* isomerization of the K116−P117 bond (*18*). Apparently, [W140A]SNase(111−143) is incapable of structurally complementing SNase121. This may because the substitution of tryptophan with alanine removes the aromatic side chain at position 140 of SNase(111−143), and changes the local structure suitable for W140. When W140 was substituted by a phenylalanine, the [W140F]SNase(111−143) can restore 9% nuclease activity to mixture (Table 1). Moreover, SNase121 has different partially folded conformations upon mixing with [W140F]SNase(111−143) as shown by the 2D HSQC spectrum of SNase121 in the complex (Figure 8C in the Supporting Information). When the concentration of [W140F]SNase(111−143) was increased and reached a 1:2 molar ratio of SNase121/[W140F]SNase(111−143), the 2D $^{1}H-^{15}N$ HSQC spectrum of SNase121 in the complex showed only one cross peak for each of G29, K70, and D95 (Figure 8D in the Supporting Information), indicating stabilized conformation of SNase121 in the complex. However, broad resonances in the center of the spectrum of SNase121 in the complex indicated that the capability of structural complementation of [W140F]SNase(111−143) to SNase121 is lower. Probably, the aromatic side chain of phenylalanine cannot fit well the local structure of residue 140 in the complex. On the other hand, the cation−π interactions between the aromatic side chain and cationic side chain of Lys or Arg contribute largely to protein folding and stability alongside the hydrophobic interactions, and Trp is the most likely of the aromatics to be involved in a cation−π interaction (*44*). The detected cation−π interactions between W140−K133 and W140−K110 in the SNase121:SNase(111−143) complex (Table 3 in the Supporting Information) should play an important role in recognition of the two fragments. Therefore, W140 of SNase(111−143) is essential to permit the high efficiency of complementation of SNase(111−143) to SNase121, and the complementation of these two fragments appears to be very sensitive to the local structural details at sequence position of 140.

(*c*) *Stable Native-like Conformation of the Helix* α_3 *in SNase*(*111*−*143*) *Is Required for Recognition Process*. SNase(111−143) contains a sequence region (E122−K136) constructing the helix α_3 of native SNase. E129 and K133 are the two residues located on the same face of the helix α_3 in the structure of native SNase. As was indicated, the side-chain to side-chain lactam bridge of (i, i + 4) spaced residues glutamic-lysine can induce or stabilize helical structure in peptides (*45*, *46*). Actually, characteristic of a nascent helix was observed for peptide corresponding to residues E129−E142 of SNase in aqueous solution (*47*). This implies that the interactions between the side chains of E129 and K133 in SNase(111−143) could stabilize the helical structure in the corresponding segment. The E129A mutation of SNase(111−143) destroyed this lactam bridge, resulting in destabilization of the helix conformation. As a result, only 9% of native nuclease activity can be obtained for the mixture of SNase121 and [E129A]SNase(111−143) (Table 1). The 2D $^{1}H-^{15}N$ HSQC spectra obtained for SNase121 in the mixture with [E129A]SNase(111−143) (Figure 9 in the Supporting Information) demonstrate similar features as observed for SNase121 in the mixture with [W140F]SNase(111−143) (Figure 8C,D in the Supporting Information). In addition, E122 and R126 are the two residues located on the same face of the helix α_3, and the ionic interactions between the side chains of E122 and R126 (*43*) can also play a role in stabilizing the structure of the helix α_3 in native SNase. E122A or R126L mutations may destroy the native-like interactions between them and destabilize the helix conformation in SNase(111−143), giving only 10% of native nuclease activity in the complex (Table 1). Therefore, a stable native-like conformation of the helix α_3 in SNase(111−143) is required for recognition process of SNase121 and SNase(111−143).

Interaction-Induced Structural Complementation of the Two SNase Fragments. (*a*) *Native-like Tertiary Interactions at the Binding Interface*. As is shown by the above analysis, the tight association of SNase121 with SNase(111−143) in forming a stable complex is sensitive to the crucial elements in the three surface regions of the binding interface between the two fragments. It is likely that the crucial native-like tertiary interactions between the residues of these elements are involved in the fragment recognition process and in the stabilization of the complex.

In the first surface region of the binding interface, the intermolecular NOEs between residues N118−T120 of SNase(111−143) and residues D77−G79 of SNase121 were identified in the SNase121:SNase(111−143) complex (Tables 1 and 2 in the Supporting Information). Actually, residues P117−T120 of the A112−H121 loop are coupled with residues D77−Q80 of the p-loop through N118Oδ_1−G79N, N118Nδ_2−Q80O, T120OG1−D77OD2, and T120N−D77OD1 hydrogen-bonding interactions in native SNase (*43*). Therefore, the intermolecular interactions between residues N118−T120 of SNase(111−143) and residues D77−G79 of SNase121 should contribute to the functional complementation of the two fragments. This is supported by the mutations of residues N118−T120 in SNase(111−143). The N118G, N119G, and T120A mutant SNase(111−143) reduced the nuclease activities of the corresponding complexes compared to that of the SNase121:SNase(111−143) complex, having nuclease activities of 12%, 12%, and 17%, respectively, of the activity of the native level (Table 1). It implies that the native-like tertiary interactions could be established between residues N118−T120 of SNase(111−143) and residues D77−G79 of the p-loop of SNase121 in the first surface region of the binding interface in the complex.

In the second surface region of the binding interface, the intermolecular NOEs of residues from the helix α2 and strand β8 in SNase121 with residues from helix α3 in SNase(111−143) were identified in the complex (Tables 1 and 2 in the Supporting Information). Besides, mutation of residues S128, E129, and E135 from helix α3 of SNase(111−143) results in the reduction of both the nuclease activities of the mutant complexes (Table 1) and the efficiency of the fragment complementation as shown by the corresponding 2D $^{1}H-^{15}N$ HSQC spectra of SNase121 in the mixture with [E129A]SNase(111−143) (Figure 9 in the Supporting Information) and with [E135A]SNase(111−143) (Figure 10 in the Supporting Information). It would appear from this information that some type of interchain interactions exists in the noncovalent SNase121:SNase(111−143). As was shown, the hydrogen-bonding interactions of residues S128, E135, and E129 from the helix α3 with residues E101 and R105 from the helix α2 and residue V111 from the strand β8, respectively, contribute greatly to the stabilization of the folding of both helices α3 and α2 in the native SNase (*48*). Therefore, it is likely that the recovering of the stable conformations of both the helices α3 and α2 in the complex is contributed by native-like tertiary interactions between the helices α3 and α2 and the strand β8 at the binding interface of the SNase121:SNase(111−143) complex.

In the third surface region of the binding interface, residues L137, I139 and W140 from the C-terminal loop L137−D143 of SNase(111−143) are in close contact with residues Q106, G107, L108, and K110 from SNase121. Besides, the intermolecular NOE between residues N138 of SNase(111−143) and Y54 connecting to the N-terminal of helix α2 in SNase121 was determined (Tables 1 and 2 in the Supporting Information). This implies that a native-like local structure of W140 may exist in the complex (Figure 5C). In the native SNase, the stacking interactions between the pyrrole ring of W140 and the surrounding hydrophobic residues play a crucial role in anchoring the C-terminal small α-subdomain on the N-terminal large β-subdomain (*48*, *49*). Moreover, the side chains of N138 and S141 form hydrogen bonds with residues Q106 and Y54, respectively, in the native SNase (*48*), which may play a role in maintain the local structure of W140 and, therefore, the proper hydrophobic environment for W140. For SNase121:SNase(111−143) complex, the nuclease activity was reduced not only by mutation of W140 but also by mutations of N138 and S141 in SNase(111−143). The substitution of glycine and alanine for asparagine and serine at positions of 138 and 141, respectively, may disturb the native-like local structure of W140, and further disturb the native-like interactions of W140 with hydrophobic residues in this local structural region of the complex, resulting in the reduction of the enzyme activity (Table 1). Therefore, the native-like hydrophobic stacking interactions of W140 from SNase(111−143) with surrounding residues from both fragments serve as an anchoring force for specific association of SNase121 and SNase(111−143) in the complex.

(*b*) *Mechanism of Achieving a Structural Complementation of the Two Fragments*. As is revealed by the analysis of the experimental data, formation of the stable SNase121:SNase(111−143) noncovalent complex occurred through an early suggested folding-on-binding event (*9*). The intrinsic native-like structural propensity of SNase121 and SNase(111−143) plays a role in such a refolding event. As was reported previously, the inherent native-like tertiary interactions persist in SNase121, and

SNase121 has the intrinsic tendency to form a native-like β-barrel conformation in aqueous solution. Amino acid substitutions enhancing the local hydrophobic interactions can drive SNase121 to fold into a native-like β-subdomain (*18*). SNase(111−143) has a low conformational preference for helix structure. The amino acid composition of segment E122−K136 shows high intrinsic helical propensity (*20*), and a helix-turn conformation of the peptide E129−E142 similar to that in native SNase can be induced by 30−40% 2,2,2-trifluoroethanol (*47*). Clearly, the two individual fragments can refold to the native-like structures by promoting the inherent local or nonlocal native-like interactions which persist in the fragments. Therefore, the refolding events of the two fragments possessing the conformational preference for native-like structures would benefit from the native-like long-range interactions at the binding interface between the two fragments. In other words, the native-like tertiary interactions at the binding interface induce structural complementation of the two SNase fragments. On the other hand, the native-like interactions at the binding interface between SNase121 and SNase(111−143) are established through transient contact of the residues from both fragments in the recognition process. Residues involved in the native-like interactions require a local environment similar to that in native SNase. Changing the amino acid type or removing some residues in such a local environment largely influences the establishment of the native-like interactions, and further the structural complementation. This can be seen in the discussion of the crucial elements for structural complementation. Apparently, the increasing specific native-like conformations and establishing the native-like interactions at the binding interface are the two concomitant processes.

Like SNase121 and SNase(111−143), all the early reported SNase fragments isolated from trypsin digests for complementation study (*1*, *11*−*14*) possess the potential local or nonlocal nucleation sites and the intrinsic native-like structural propensity for "β-barrel" structure, β-sheet-like structure, or α-helix (*18*, *20*, *50*). Since the intrinsic local and nonlocal interactions in these potential nucleation sites are insufficient to stabilize the folding of the fragment due to the shortage of relevant long-range interactions from other part of the protein, the association of the complementary fragments generates the additional long-range interactions facilitating the stabilized folding of the fragments.

From the above analysis, fragments SNase121 and SNase(111−143) can achieve highly efficient structural complementation because they fulfill two requirements: First, the two fragments have intrinsic structural propensity; second, the two fragments provide necessary sequence elements for recognition at the binding interface between them. The elements essential for recognition and efficient complementation of the two fragments are also crucial for establishing the native-like interactions at the binding interface of the complex. The structural complementation is induced by the native-like long-range interactions between the two complementary fragments. In consequence, the interfragment interactions that induce the structural complementation of SNase121 and SNase(111−143) likely reflect the tertiary interactions necessary to stabilize the folding of both β- and α-subdomains in the native SNase.

SUPPORTING INFORMATION AVAILABLE

Ten figures and two tables. This material is available free of charge via the Internet at http://pubs.acs.org.

REFERENCES

1. Taniuchi, H., Anfinsen, C. B., and Sodja, A. (1967) Nuclease-T: an active derivative of staphylococcal nuclease composed of two noncovalently bonded peptide fragments. *Proc. Natl. Acad. Sci. U.S.A. 58*, 1235–1242.
2. Schmidt-Rose, T., and Jentsch, T. J. (1997) Reconstitution of functional voltage-gated chloride channels from complementary fragments of CLC-1. *J. Biol. Chem. 272*, 20515–20521.
3. Braun, M., Endriss, F., Killmann, H., and Braun, V. (2003) In vivo reconstitution of the FhuA transport protein of *Escherichia coli* K-12. *J. Bacteriol. 185*, 5508–5518.
4. Kim, B. J., Mangala, S. L., Muralidhara, B. K., and Hayashi, K. (2007) Fragment complementation for the co-refolding of *Thermotoga maritima* beta-glucosidase by gene splitting at non-homologous region. *Enzyme Microb. Technol. 40*, 732–739.
5. Richards, F. M., and Vithayathil, P. J. (1959) The preparation of subtilisn-modified ribonuclease and the separation of the peptide and protein components. *J. Biol. Chem. 234*, 1459–1465.
6. Hartley, R. W. (1977) Complementation of peptides of barnase, extracellular ribonuclease of Bacillus amyloliquefaciens. *J. Biol. Chem. 252*, 3252–3254.
7. de Prat Gay, G., and Fersht, A. R. (1994) Generation of a family of protein fragments for structure-folding studies. 1. Folding complementation of two fragments of chymotrypsin inhibitor-2 formed by cleavage at its unique methionine residue. *Biochemistry 33*, 7957–7963.
8. Williams, K. P., and Shoelson, S. E. (1993) Cooperative self-assembly of SH2 domain fragments restores phosphopeptide binding. *Biochemistry 32*, 11279–11284.
9. Ojennus, D. D., Fleissner, M. R., and Wuttke, D. S. (2001) Reconstitution of a native-like SH2 domain from disordered peptide fragments examined by multidimensional heteronuclear NMR. *Protein Sci. 10*, 2162–2175.
10. Sun, Y. C., Li, Y., Zhang, H., Yan, H. Q., Dowling, D. N., and Wang, Y. P. (2006) Reconstitution of the enzyme AroA and its glyphosate tolerance by fragment complementation. *FEBS Lett. 580*, 1521–1527.
11. Taniuchi, H., and Anfinsen, C. B. (1968) Steps in the formation of active derivatives of staphylococcal nuclease during trypsin digestion. *J. Biol. Chem. 243*, 4778–4786.
12. Taniuchi, H., and Anfinsen, C. B. (1969) An experimental approach to the study of the folding of staphylococcal nuclease. *J. Biol. Chem. 244*, 3864–3875.
13. Taniuchi, H., and Anfinsen, C. B. (1971) Simultaneous formation of two alternative enzymology active structures by complementation of two overlapping fragments of staphylococcal nuclease. *J. Biol. Chem. 246*, 2291–2301.
14. Andria, G., Taniuchi, H., and Cone, J. L. (1971) The specific binding of three fragments of staphylococcal nuclease. *J. Biol. Chem. 246*, 7421–7428.
15. Taniuchi, H., Parker, D. S., and Bohnert, J. L. (1977) Study of equilibration of the system involving two alternative, enzymically active complementing structures simultaneously formed from two overlapping fragments of staphylococcal nuclease. *J. Biol. Chem. 252*, 125–140.
16. Taniuchi, H., Davies, D. R., and Anfinsen, C. B. (1972) A comparison of the x-ray diffraction patterns of crystals of reconstituted nuclease-T and of native staphylococcal nuclease. *J. Biol. Chem. 247*, 3362–3364.
17. Xie, T., Liu, D., Feng, Y., Shan, L., and Wang, J. (2007) Folding stability and cooperativity of the three forms of 1−110 residues fragment of staphylococcal nuclease. *Biophys. J. 92*, 2090–2107.
18. Feng, Y., Liu, D., and Wang, J. (2003) Native-like partially folded conformations and folding process revealed in the N-terminal large fragments of staphylococcal nuclease: a study by NMR spectroscopy. *J. Mol. Biol. 330*, 821–837.
19. Ye, K., Jing, G., and Wang, J. (2000) Interactions between subdomains in the partially folded state of staphylococcal nuclease. *Biochim. Biophys. Acta 1479*, 123–134.
20. Geng, Y., Wang, M., Xie, T., Feng, Y., and Wang, J. (2007) Folding of the C-terminal fragment V111-D143 of staphylococcal nuclease in aqueous solution. *Protein Pept. Lett. 14*, 747–755.
21. Cuatrecasas, P., Fuchs, S., and Anfinsen, C. B. (1967) Catalytic properties and specificity of the extracellular nuclease of *Staphylococcus aureus*. *J. Biol. Chem. 242*, 1541–1547.
22. Viguera, A. R., Arrondo, J. L., Musacchio, A., Saraste, M., and Serrano, L. (1994) Characterization of the interaction of natural proline-rich peptides with five different SH3 domains. *Biochemistry 33*, 10925–10933.
23. Schmidt, H., Hoffmann, S., Tran, T., Stoldt, M., Stangler, T., Wiesehan, K., and Willbold, D. (2007) Solution structure of a Hck

SH3 domain ligand complex reveals novel interaction modes. *J. Mol. Biol. 365*, 1517–1532.
24. Sattler, M., Schleucher, J., and Griesinger, C. (1999) Heteronuclear multidimensional NMR experiments for the structure determination of proteins in solution employing pulsed field gradients. *Prog. Nucl. Magn. Reson. Spectrosc. 34*, 93–158.
25. Yamazaki, T., Muhandiram, R., and Kay, L. E. (1994) NMR experiments for the measurement of carbon relaxation properties in highly enriched, uniformly ^{13}C,^{15}N-Labeled Proteins: Application to $^{13}C_{\alpha}$ Carbons. *J. Am. Chem. Soc. 116*, 8266–8278.
26. Farrow, N. A., Zhang, O., Forman-Kay, J. D., and Kay, L. E. (1994) A heteronuclear correlation experiment for simultaneous determination of ^{15}N longitudinal decay and chemical exchange rates of systems in slow equilibrium. *J. Biomol. NMR. 4*, 727–734.
27. Viles, J. H., Duggan, B. M., Zaborowski, E., Schwarzinger, S., Huntley, J. J., Kroon, G. J., Dyson, H. J., and Wright, P. E. (2001) Potential bias in NMR relaxation data introduced by peak intensity analysis and curve fitting methods. *J. Biomol. NMR 21*, 1–9.
28. Hall, J. B., and Fushman, D. (2006) Variability of the ^{15}N chemical shielding tensors in the B3 domain of protein G from ^{15}N relaxation measurements at several fields. Implications for backbone order parameters. *J. Am. Chem. Soc. 128*, 7855–7870.
29. Dosset, P., Hus, J. C., Blackledge, M., and Marion, D. (2000) Efficient analysis of macromolecular rotational diffusion from heteronuclear relaxation data. *J. Biomol. NMR 16*, 23–28.
30. Pawley, N. H., Wang, C., Koide, S., and Nicholson, L. K. (2001) An improved method for distinguishing between anisotropic tumbling and chemical exchange in analysis of ^{15}N relaxation parameters. *J. Biomol. NMR 20*, 149–165.
31. Cordier, F., Caffrey, M., Brutscher, B., Cusanovich, M. A., Marion, D., and Blackledge, M. (1998) Solution structure, rotational diffusion anisotropy and local backbone dynamics of *Rhodobacter capsulatus* cytochrome c2. *J. Mol. Biol. 281*, 341–361.
32. Tjandra, N., Feller, S. E., Pastor, R. W., and Bax, A. (1995) Rotational diffusion anisotropy of human ubiquitin from ^{15}N NMR relaxation. *J. Am. Chem. Soc. 117*, 12562–12566.
33. Cornilescu, G., Delaglio, F., and Bax, A. (1999) Protein backbone angle restraints from searching a database for chemical shift and sequence homology. *J. Biomol. NMR 13*, 289–302.
34. Brunger, A. T., Adams, P. D., Clore, G. M., DeLano, W. L., Gros, P., Grosse-Kunstleve, R. W., Jiang, J. S., Kuszewski, J., Nilges, M., Pannu, N. S., Read, R. J., Rice, L. M., Simonson, T., and Warren, G. L. (1998) Crystallography & NMR system: A new software suite for macromolecular structure determination. *Acta Crystallogr., Sect. D: Biol. Crystallogr. 54*, 905–921.
35. Linge, J. P., Williams, M. A., Spronk, C. A., Bonvin, A. M., and Nilges, M. (2003) Refinement of protein structures in explicit solvent. *Proteins 50*, 496–506.
36. Nederveen, A. J., Doreleijers, J. F., Vranken, W., Miller, Z., Spronk, C. A. E. M., Nabuurs, S. B., Guntert, P., Livny, M., Markley, J. L., Nilges, M., Ulrich, E. L., Kaptein, R., and Bonvin, A. M. J. J. (2005) RECOORD: A recalculated coordinate database of 500+proteins from the PDB using restraints from the BioMagResBank. *Proteins 59*, 662–672.
37. Koradi, R., Billeter, M., and Wüthrich, K. (1996) MOLMOL: A program for display and analysis of macromolecular structures. *J. Mol. Graphics 14*, 51–55.
38. Laskowski, R. A., Rullmann, J. A. C., MacArthur, M. W., Kaptein, R., and Thornton, J. M. (1996) AQUA and PROCHECK-NMR: Programs for checking the quality of protein structures solved by NMR. *J. Biomol. NMR 8*, 477–486.
39. Laskowski, R. A., Rullmannn, J. A., MacArthur, M. W., Kaptein, R., and Thornton, J. M. (1996) AQUA and PROCHECK-NMR: programs for checking the quality of protein structures solved by NMR. *J. Biomol. NMR 8*, 477–486.
40. Lipari, G., and Szabo, A. (1982) Model-free approach to the interpretation of nuclear magnetic resonance relaxation in macromolecules. 1. Theory and range of validity. *J. Am. Chem. Soc. 104*, 4546–4559.
41. Mandel, A. M., Akke, M., and Palmer, A. G.3rd. (1995) Backbone dynamics of *Escherichia coli* ribonuclease HI: correlations with structure and function in an active enzyme. *J. Mol. Biol. 246*, 144–163.
42. Wang, J., Truckses, D. M., Abildgaard, F., Dzakula, Z., Zolnai, Z., and Markley, J. L. (1997) Solution structures of staphylococcal nuclease from multidimensional, multinuclear NMR: nuclease-H124L and its ternary complex with Ca^{2+} and thymidine-3′,5′-bisphosphate. *J. Biomol. NMR 10*, 143–164.
43. Hynes, T. R., and Fox, R. O. (1991) The crystal structure of staphylococcal nuclease refined at 1.7 Å resolution. *Proteins 10*, 92–105.
44. Gallivan, J. P., and Dougherty, D. A. (1999) Cation-pi interactions in structural biology. *Proc. Natl. Acad. Sci. U.S.A. 96*, 9459–9464.
45. Mierke, D. F., Maretto, S., Schievano, E., DeLuca, D., Bisello, A., Mammi, S., Rosenblatt, M., Peggion, E., and Chorev, M. (1997) Conformational studies of mono- and bicyclic parathyroid hormone-related protein-derived agonists. *Biochemistry 36*, 10372–10383.
46. Houston, M. E., Jr., Campbell, A. P., Lix, B., Kay, C. M., Sykes, B. D., and Hodges, R. S. (1996) Lactam bridge stabilization of alpha-helices: the role of hydrophobicity in controlling dimeric versus monomeric alpha-helices. *Biochemistry 35*, 10041–10050.
47. Maciejewski, M. W., and Zehfus, M. H. (1995) Structure of a compact peptide from staphylococcal nuclease determined by circular dichroism and NMR spectroscopy. *Biochemistry 34*, 5795–5800.
48. Hirano, S., Mihara, K., Yamazaki, Y., Kamikubo, H., Imamoto, Y., and Kataoka, M. (2002) Role of C-terminal region of staphylococcal nuclease for foldability, stability, and activity. *Proteins 49*, 255–265.
49. Hirano, S., Kamikubo, H., Yamazaki, Y., and Kataoka, M. (2005) Elucidation of information encoded in tryptophan 140 of staphylococcal nuclease. *Proteins 58*, 271–277.
50. Wang, X., Wang, M., Tong, Y. F., Shan, L., and Wang, J. F. (2006) Probing the folding capacity and residual structures in 1−79 residues fragment of staphylococcal nuclease by biophysical and NMR methods. *Biochimie 88*, 1343–1355.